2024 IEEE International Conference on Robotics and Automation (ICRA 2024)
May 13-17, 2024. Yokohama, Japan

A soft miniaturized continuum robot with 3D shape sensing via functionalized soft optical waveguides

Viola Del Bono, Max McCandless, Frank Julia Wise, and Sheila Russo‡

***Abstract*— In this paper, we present a fully soft miniaturized continuum robot that integrates 3D optical shape sensing through functionalized tubing used as soft optical waveguides. The sensor is fabricated by laser patterning an off-the-shelf medical tubing, allowing for bidirectional responses to large curvatures in two bending directions, enabling 3D shape sensing and tip tracking of the continuum robot. The robot is able to bend and sense its own shape up to a curvature of 44.7 m^{-1}, corresponding to a bending angle of 102°, having high-accuracy tracking capabilities, resulting in an average tracking error of 3.08 mm, that is 7.7 % of the robot length. The robot's functionality was shown in validation experiments, including a real-time shape prediction through a graphical user interface.**

I. Introduction

In the evolving landscape of robotics, soft robots stand as a promising alternative to their traditional rigid counterparts [1], [2]. Drawing inspiration from the inherent flexibility and adaptability of natural organisms, these systems are able to continuously deform with an infinite number of degrees of freedom [3], [4]. Due to their large body length to cross-section diameter ratio, or slenderness, soft continuum robots are uniquely suited to tasks that require the deployment of tools into tortuous and narrow paths, and present a high degree of compliance when interacting with objects [2]. Besides enhancing flexibility and compliance, they bring other numerous advantages, such as safety, lightweight, versatile design and actuation, simplified control, and adaptation to unstructured environments [5]–[7]. These aspects enable a variety of applications, ranging from inspection and repair in aerospace [8], [9], search and rescue in hazardous environments [10], [11], underground exploration [12], [13], object manipulation [14], [15], to medical applications, such as wearable devices [16]–[18], minimally invasive surgery (MIS), and endoscopic procedures [19]–[23].

Due to the intricate and delicate nature of surgical procedures and the need for safe and gentle interactions with tissues and organs, MIS and endoscopy are particularly promising applications for soft continuum robots [24]–[27]. However, robots need to be scaled down to a millimeter scale to navigate through the human body, thus increasing their design and manufacturing complexity and system component integration difficulty [28]. Moreover, surgeons rely on their tactile senses and visual cues to make informed decisions during traditional surgery. Replicating these sensing capabilities in a robotic system, along with providing real-time information, such as force feedback, tissue properties, or shape sensing, is a challenge that requires advanced sensing technologies and control algorithms [24], [29]. By exploiting magnetic actuation, soft miniaturized catheters have been developed [30]–[33]. However, they do not integrate sensing, thus they cannot be controlled in closed-loop.

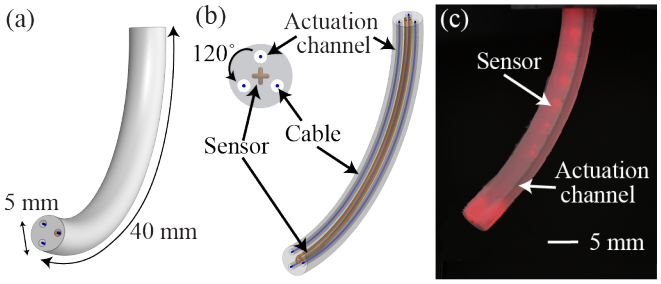

Fig. 1. A soft miniaturized continuum robot with 3D shape sensing via functionalized soft optical waveguides. a) External view of the robot body. b) Internal and section view of the robot. The sensor loops are running along the body in an orthogonal configuration. The three actuation channels are spaced 120° apart and the cables are running inside them. c) A picture of the fabricated robot while bending. The sensor and actuation channel are visible inside the robot body.

A variety of soft sensing technologies are available today, both for proprioception and exteroception, but there is still a gap to effectively utilize them in soft robots for MIS applications, mainly due to challenges in size, high number of sensors needed, wiring, system integration, and lack of biocompatibility [34]. Stretchable strain sensors based on resistive and piezoresistive technologies have been integrated in soft actuators to sense curvature and elongation, including conductive liquid metals [35]–[37], ionic fluids [38]–[40], conductive polymer nanocomposites [41], [42] and yarns [43], [44]. These types of sensors, however, have limited sensitivity, large hysteresis and temperature drift. Soft capacitive sensors have been developed for tactile sensing [45]–[47], but they are very sensitive to the environment and require shielding techniques, that increases fabrication complexity. Magnetic sensors have also been proposed for soft robotic skins [48], [49] and curvature sensing [50], [51]. They are a promising approach, but vulnerable to external magnetic interactions. Optical sensors such as FBGs (Fiber Bragg Grating) [52], [53] and FOSSs (Fiber Optic Sensing System) [54] have also been proposed for shape sensing of continuum robots. However, these technologies present limitations such as high cost, manufacturing complexity, limited stretchability, and bulky electronics, hampering their applications in soft continuum robots [55], [56]. Soft optical

The authors are with the Department of Mechanical Engineering, Boston University, Boston, Massachusetts 02215.
‡Corresponding author. E-mail: russos@bu.edu.

sensors are a promising emerging approach since they are highly deformable, low cost, intrinsically safe, immune to electromagnetic interferences, easy to fabricate, and versatile in their design [57], [58]. They have been mainly used for curvature sensing [59], [60], tactile sensing [61], and contact force detection [62], [63].

This paper presents a fully soft, miniaturized continuum robot that integrates 3D optical shape sensing through functionalized soft optical sensors (Fig. 1). The robot can steer in all directions via three cables running through three actuation channels. It features two U-shaped soft optical sensors placed in an orthogonal cross configuration. The soft optical sensor is created through a laser precision machining functionalization technique performed on a commercial off-the-shelf medical tubing, resulting in a simple, low-cost, versatile sensing solution with a potential of multiple applications in soft robotics. Each optical sensor is able to sense the degree and also the direction of bending, represented by changes in optical power (i.e., optical gain and optical loss), thanks to a selective patterning of its surface.

II. Materials and Methods

A. Soft Robot Design

The soft continuum robot diameter is 5 mm, and its length is 40 mm (Fig. 1, a). Three actuation channels with a 1 mm diameter are spaced 120° apart, with a distance from the center of the robot of 1.75 mm (Fig. 1, b). The two perpendicular optical sensors have a radius of curvature of 0.5 mm in correspondence with their U-shaped section. Their cross section is 3.142 mm^2. Each sensor consists of a functionalized optically clear polyurethane medical tubing (Micro-Renathane©, Braintree Scientific) with an external diameter of 0.635 mm and internal diameter of 0.305 mm. The tube works as an optical waveguide with the core being the polyurethane tube material itself, the external cladding being the surrounding Dragon Skin© 10 MEDIUM (Smooth-On), and the internal cladding being air. Two red 650 nm LEDs (IF-E99B, Industrial Fiber Optics) are utilized as light source emitters, while two photo-transistors (IF-D92, Industrial Fiber Optics) are used as receivers to read the sensor signal. A picture of the robot is shown in Figure 1, c.

B. Soft Robot Fabrication

The fabrication process consists of two main steps: first, the sensor fabrication, and then the integration of the sensor into the soft continuum robot body.

1) Sensor fabrication: Two 40 cm sections of tubing are used as waveguides. A laser (Coherent Matrix 355 nm laser precision micromachining system, 5 W) is used to functionalize the tubing by patterning its surface via the creation of six V-shaped cuts. Only one side of the tube surface is functionalized with cuts spaced 4 mm apart and with a depth of 0.3175 mm, that is half of the tube diameter. This results in a patterned length of 20 mm (Fig. 2, a). In order to place the tubes in a cross-configuration, two soft aligners are firstly fabricated by pouring Dragon Skin© 10 MEDIUM (Smooth-On) mixed with 10% by weight OS-2 solvent (DowSil, Dow Inc.) into 3D printed molds, degassed, and placed in oven to cure at 70°C for 10 min (Fig. 2, b). The aligners contain four holes each to accommodate the waveguides and their aim is to maintain the two loops in place. After removing the extra material needed from de-molding the two aligners, each waveguide is looped into them, making sure that the two patterned surfaces are orthogonal to each other (Fig. 2, c).

2) Soft continuum robot body fabrication: Four 0.254 mm stainless steel rods are inserted into each of the four waveguide ends as a core support for the next molding step. This maintains the sensor in position and prevents silicone from entering the cuts during the subsequent molding. The mold for the robot body consists of two 3D printed halves of a 5 mm cylinder printed on (Formlabs©, Form 2). It has two interchangeable end caps with three holes for accommodating 1 mm pins that will create the actuation channels. In the front end cap an additional central hole of 1.65 mm provides an exit for the sensor tubing (Fig. 2, d). Having interchangeable end caps is advantageous since it allows to quickly change the robot design by keeping the cylindrical mold and re-printing only the end caps. Once the sensor is placed in the mold and the pins are inserted, Dragon Skin© 10 MEDIUM (Smooth-On) mixed with 10% by weight OS-2 solvent (DowSil, Dow Inc.) is poured into the two halves of the mold. They are degassed, sandwiched together, and cured in oven at 70°C for 10 min. The rods and the pins are then pulled out and the continuum robot is de-molded. Three cables of 0.3 mm diameter are inserted in each channel, and secured at the tip of the robot with adhesive (Fig. 2, e). The larger size of the actuation channels, with respect to the cables, reduced friction between the latter and the robot silicone body.

C. Sensor working principle

According to optical theory, light travels in an optical waveguide by total internal reflection. When deformed (i.e., bending, stretching, or applying contact force), the optical output power (light intensity) of a waveguide will be altered. This optical power loss P is calculated from the baseline signal in an undeformed state I_0 and the measured signal I as:

$$P = 10 \log (I_0/I). \tag{1}$$

In order to be used as a curvature sensor, the incident angle of the reflected light needs to change with bending; this, in turn, causes the measured light intensity to change. In an isotropic and symmetrically shaped waveguide, this alteration usually results in a loss of signal with respect to its baseline (I_0) in a straight configuration due to some light rays reflecting off the interface of the materials making up the waveguide at an angle less than the angle of total internal reflection θ_c, as defined by Eq. 2:

$$\theta_{\mathrm{c}} = sin^{-1}(n_{\mathrm{b}}/n_{\mathrm{a}}) \tag{2}$$

where n_b is the refractive index (RI) of the cladding material of the waveguide and n_a is the core material RI. The core is the medium the light travels through and the cladding is the medium surrounding the core that makes up the optical

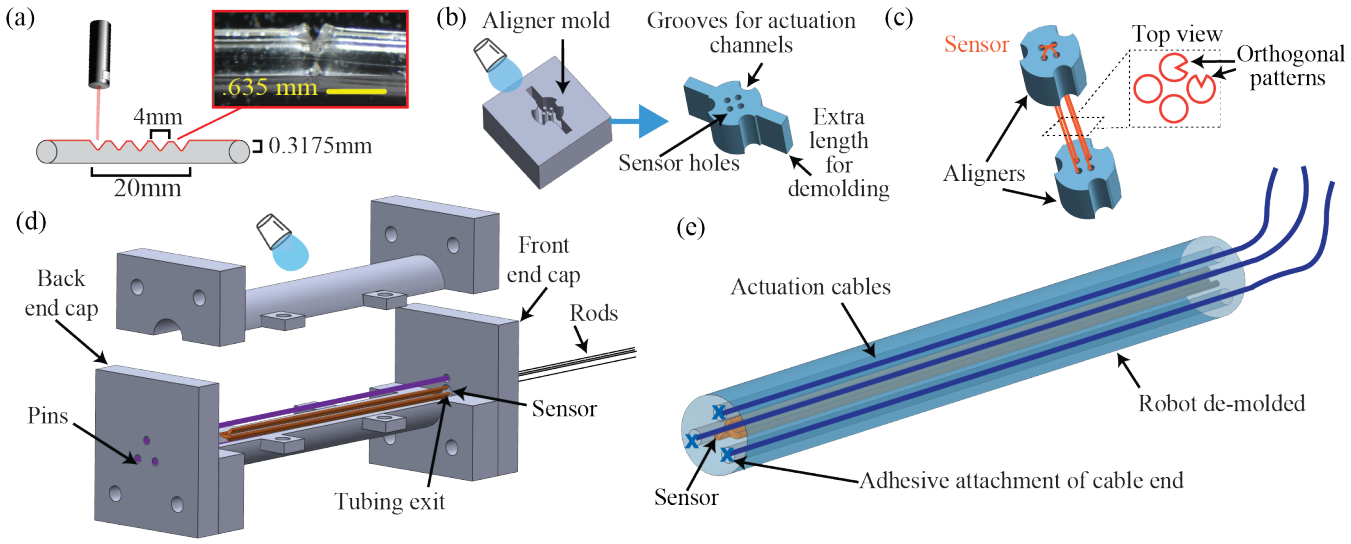

Fig. 2. Fabrication of the soft continuum robot. a) Laser patterning of the upper surface of the sensor producing V-shaped cuts. b) Two aligners are molded by pouring silicone into a 3D printed mold. The aligners have grooves for accommodating the actuation pins and four holes for accommodating the sensor tubing. c) After removing the extra material needed for de-molding the aligners, the sensor is looped inside them, placing the patterned surfaces orthogonal to each other. d) Three stainless steel rods are inserted into the sensor and the latter is placed inside the continuum robot mold, along with three pins for the actuation channels. Silicone is poured into the two halves of the mold and, after degassing, they are sandwiched together, and cured. e) The continuum robot is removed from the mold. Three cables are inserted into the actuation channels, and secured at the robot tip with adhesive.

interface that the light interacts with by reflecting off of, transmitting through, or being absorbed by the cladding material. Internal reflection can occur when $n_a > n_b$ and a larger disparity between the RIs will mean that θ_c is smaller and thus will mean that more of the light is totally internally reflected, on average. It follows that the larger disparity between the RIs will mean that the sensors are less prone to bending losses due to the fact that bending losses occur due to changing the angle of the incident light on the sensors; however, in the case of smaller θ_c, even large changes to the incident light angle will still allow for total internal reflection to occur. If an anisotropy is introduced only on one side of the waveguide surface, the waveguides sensitivity to bending (curvature changes) can be more easily monitored. Further, two different responses can be obtained depending on the direction of bending if the sensors are manufactured selectively.

In this paper, we introduce anisotropy by selectively patterning the tubing upper surface via laser precision micromachining, creating a series of V-shaped cuts, as shown in Fig. 3, a, (right). Rather than a waveguide consisting of only two materials ($n_a = n_{core}$ and $n_b = n_{cladding}$), the fabrication results in the waveguide core ($n_2 = n_{tubing}$) being interfaced with two separated cladding materials ($n_1 = n_{air}$ and $n_3 = n_{silicone}$ [Dragon Skin© 10 MEDIUM]), as shown in Fig. 3, a, (left). Fig. 3, b depicts the effects that the multiple cladding have on the ability of the waveguide core to pass light through it. The RI of air is $n_1 \approx 1.00$, which is significantly smaller than the polyurethane tubing ($n_2 \approx 1.67$) and the silicone cladding material ($n_3 \approx 1.41$) (the cladding material RIs are estimated based on the RI of similar materials and quantified in order to further explain

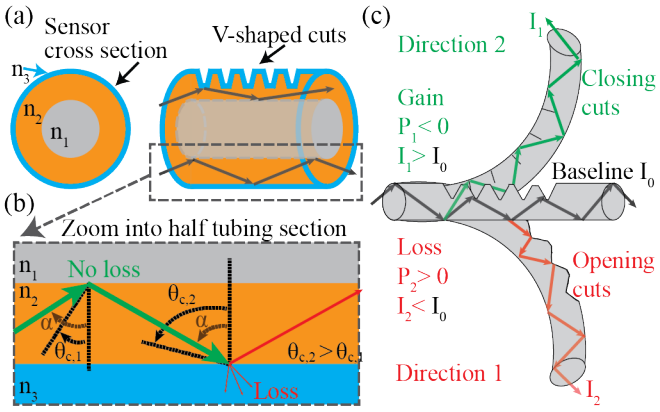

Fig. 3. Physical principle of the soft optical sensor. a) Tube waveguide cross section showing the core material (n_2) surrounded by a silicone cladding (n_3) on the outside and an air cladding (n_1) on the inside of the tube as well as the patterned cuts on the top of the tube. b) A side view of the waveguide path showing the different θ_c values depending on the interface. c) A diagram of the patterned cuts effect on the light traveling through the waveguide. In an unbent configuration (I_0), the baseline signal traverses the optical path with minimal light intensity losses. When bent in direction 2, the cuts close, and the optical signal increases as compared to direction 1, wherein the cuts open further and optical loss occurs.

the physics related to the critical angle of total internal reflection) [64], [65]. This means that the interface between the core material and the two mediums will have different θ_c, as shown in Fig. 3, b. In Fig. 3, b, we see that a light ray with an angle of incidence of α with respect to the interface will be totally internally reflected when the cladding material is air ($\alpha > \theta_{c,1}$) but only be partially reflected when interacting with the silicone cladding material ($\alpha < \theta_{c,2}$). This unique waveguide (having air as an internal

cladding) causes the light rays to traverse the waveguide with high baseline signals, due to the small critical angle of the polyurethane and air interface $\theta_{c,1} \approx 36.8°$.

When the robot bends in the direction of the patterned region (Fig. 3, c), the cuts will gradually close and more light is going to be transmitted through the tube surface since its probability to escape through the cuts is decreasing as they become smaller, until closure. This leads to an increase of signal, or optical gain $P_1 < 0$ (Fig. 3, c). Moreover, the cladding material is closing as the bending occurs, meaning that the trapped light either does not travel through a different medium or scatters back into the sensor. Conversely, when the robot bends in the opposite direction, towards the un-patterned region, the cuts are going to gradually open and more light will escape through them, resulting in a decrease of signal, or optical loss $P_2 > 0$ (Fig. 3, c). Since each sensor fabricated with this patterning technique has a bidirectional response to 2D bending, in order to sense the robot shape in 3D, two sensors placed in an orthogonal configuration will provide sufficient responses to allow for unique sensor signals throughout 3D space. This, ultimately, allows for the ability to use two embedded waveguides within the body of a continuum robot to track shape and tip positions of the small-scale soft continuum robot.

III. Experiments

A. Bidirectional response test

In order to evaluate the bidirectional response of the sensor, a planar bending experiment was performed. The robot was oriented with one of the two sensors orthogonal to the testing platform. The robot's base was locked in a fixture, and its body was bent, stepping into 12 different curvatures, up to a curvature of 46.5 m^{-1}, recording the sensor data for each step, by using an Arduino. The setup is shown in Fig. 4, a. This procedure was repeated both in the direction of optical gain and optical loss. The test was subsequently performed on a robot integrating a sensor without surface patterning (i.e., an off-the-shelf medical tubing without laser functionalization) for comparison to highlight the capabilities of our patterning technique.

B. Calibration

The robot was calibrated by relating its position to the response of each of the two sensors P_1 and P_2, throughout the 3D workspace. Three servo motors (LD-220MG, Hiwonder) were connected to the three actuation cables. When the servo motors rotate, each cable can be pulled by winding on a pin, causing the robot to bend. The sensor data was collected by a DAQ (NI USB-6002), and the position of the robot tip was acquired by an Aurora electromagnetic (EM) tracker. A small EM probe was fixed at the tip of the soft robot. The test setup is shown in Fig. 5, a. All the data was synchronized and analyzed through a Python code. The robot was actuated up to a curvature of 44.7 m^{-1}, corresponding to a bending angle of 102°. The bending angle was calculated as the length of the continuum robot divided by the radius of curvature.

To model the shape of the continuum robot, a constant curvature modeling approach was utilized [66]. The tip coordinates (x, y, z) were converted into arc parameters (k, ϕ) representing the curvature and the rotation around z-axis (see Fig. 5, b). The relationship between (x, y, z) coordinates and the arc parameters is given by trigonometric functions:

$$k = 1/r \tag{3}$$

$$\phi = \tan^{-1}(y/x) \tag{4}$$

where r is the radius of curvature and it is given by $r = l/\theta$, where $\theta = f(x, y, z)$ is the bending angle (defined previously by trigonometric rules), and $l = 40\ mm$ is the length of the robot and it is constant.

C. Surface mapping

Given that each waveguide has an area of optical gain $P < 0$, and an area of optical loss $P > 0$ depending on the bending direction, from the calibration data it is possible to identify distinct sections having different combinations of the waveguides responses. In these sections, both r and ϕ were mapped as unique surfaces by using MATLAB (Mathworks, USA), as previously done in [67]. The four surface maps extracted are defined as follows:

$$S_{r_1}, S_{\phi_1} \text{ if } P_1 > 0 \text{ and } P_2 > 0 \tag{5}$$

$$S_{r_2}, S_{\phi_2} \text{ if } P_1 > 0 \text{ and } P_2 < 0 \tag{6}$$

$$S_{r_3}, S_{\phi_3} \text{ if } P_1 < 0 \text{ and } P_2 > 0 \tag{7}$$

$$S_{r_4}, S_{\phi_4} \text{ if } P_1 < 0 \text{ and } P_2 < 0 \tag{8}$$

For example, when $P_1 < 0$ and $P_2 > 0$, S_3 is the surface used, with $\phi = S_{\phi_3}(P_1, P_2)$ and $r = S_{r_3}(P_1, P_2)$. See the results of the surface mappings for the measured parameters in Sect. IV-B.

D. Accuracy test

To evaluate the accuracy of the shape sensing, the robot was programmed to automatically follow a specific path through a range of ϕ and r values. Then, the predicted position of ϕ and r was compared to the actual (true) values recorded by the EM tracker, which tracked the tip position of the robot. A small EM probe was fixed at the tip of the soft robot. Subsequently, the average error in the tip position tracking across the experiment was determined and compared to the overall length of the robot, which verifies the accuracy of the shape sensing and tracking methods utilized.

E. Validation test: real-time shape sensing

To validate the ability of the sensor to sense its shape, the robot was actuated in a section of the 3D space, and its predicted shape was plotted on a MATLAB graphical user interface (GUI) in real-time in order to display to the user the results of the sensor feedback predictions.

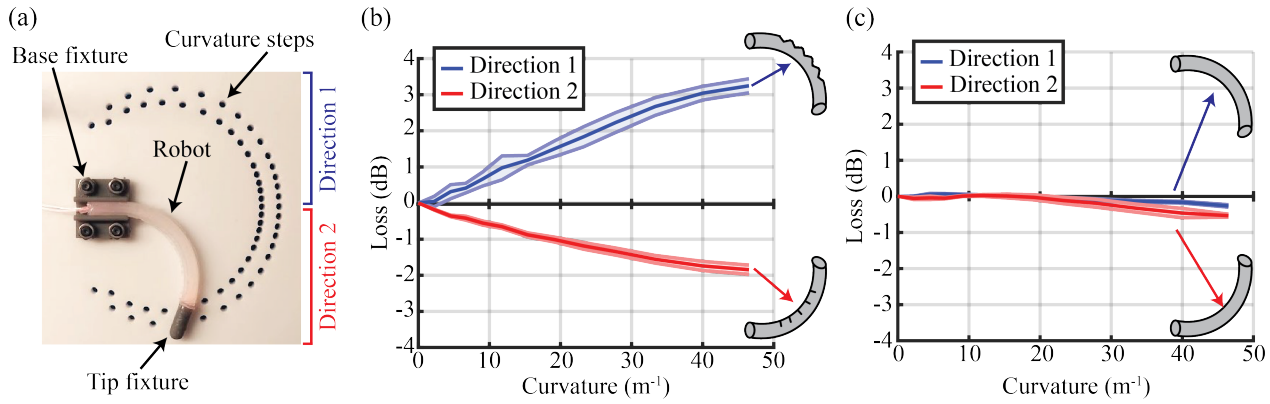

Fig. 4. Bidirectionality test. a) The experiment setup wherein the robot base is fixed and its tip is attached to a rigid mount that is inserted into the curvature slots. b) When the sensorized robot is bent in two opposite directions, there are two distinct behaviors of optical loss (blue) and optical gain (red). c) If the sensor does not have surface patterning, moving the robot in two opposite directions gives the same response, resulting in insensitivity to bending and repeated sensor responses.

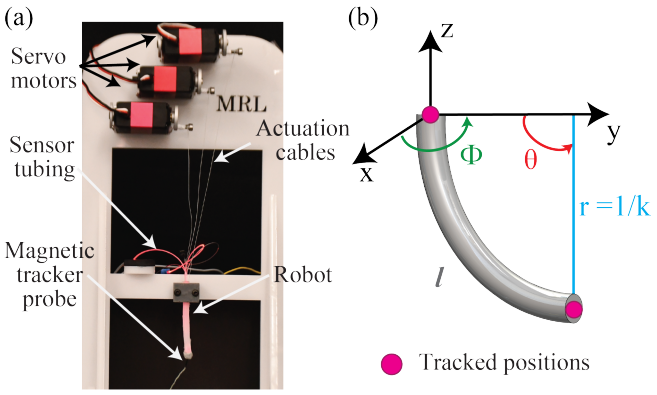

Fig. 5. Calibration of the robot workspace. a) Test setup including three servo motors connected to the actuation cables. b) Constant curvature modeling and surface fitting parameter definitions showing the tracked positions of the system (continuum robot base and tip).

IV. Results and Discussion

A. Bidirectional response test

Fig. 4 shows the performance of the patterned sensor with respect to an off-the shelf unpatterned tube. When the robot integrating the functionalized sensor is bent in two opposite directions, there are two distinct sensor responses of optical loss (Direction 1) and optical gain (Direction 2), that can be used to predict the direction of bending (Fig. 4, b), as described in Sect. II-C and Fig. 3. Conversely, a robot integrating an unpatterned tube not only has the same response for the two opposite directions, resulting in two overlapping curves, but it is also relatively insensitive to bending, since the signals do change minimally throughout the test and the optical loss measured is close to zero (Fig. 4, c). A negligible optical gain ($\approx$ -0.5 dB) can be noticed at high bending curvatures for both directions of the unpatterned tube, suggesting that our functionalization technique is necessary to achieve the desired bidirectional response of the sensor.

The bidirectional gain and loss behavior is due to two factors. Firstly, having air as the internal cladding material enables an exceptionally favorable angle of total internal reflection even at large curvatures, as shown in Eq. 2, a phenomenon not possible with other higher refractive index cladding materials. Additionally, the surfaces of the tube are highly smooth and enable the light to travel through the length of the waveguide without much optical transmission loss due to light scattering on a rougher surface interface. The functionalized soft optical waveguides, achieved with our laser patterning manufacturing approach (see Sect. II-B), exhibit unique sensor responses at all curvatures in both bending directions, allowing for two orthogonally aligned sensors to track 3D shape and tip position of the continuum robot accurately.

B. Calibration and workspace mapping

The workspace obtained from the calibration is shown in Fig. 6, a. The different colors represent the four surfaces based on the waveguides responses, see Sect. III-C, Eq. 5-8. The two polynomial surface mappings for r and ϕ used for the sensor validation are shown in Fig. 6, b and 6, c, respectively. A fifth order polynomial fit was used for both ϕ and r surface mappings. To find the best order that could map the data, a first order polynomial surface was initially calculated, and stepped up until the best R^2 errors were obtained. The R^2 errors of the fits are 0.93 for r and 0.90 for ϕ, resulting in highly accurate fittings of the data.

C. Sensing accuracy and validation experiments

In Fig. 7, a and Fig. 7, b, the predicted positions of ϕ and r, respectively, are compared to the true positions. The 3D projection of the tip position of the robot compared to the true tip position had an average error of 3.08 mm, which is 7.7% of the length of the robot (Fig. 7, c). The accuracy for ϕ decreases when the robot gets closer to the baseline position as if the robot is perfectly vertical, as visible in Fig. 7, b, both at the beginning and at the end of the test. This is due to the fact that, when r approaches infinity, ϕ is not able to be tracked.

Fig. 8 shows the real-time experiment described in Sec. III-E; starting from its baseline undeformed position

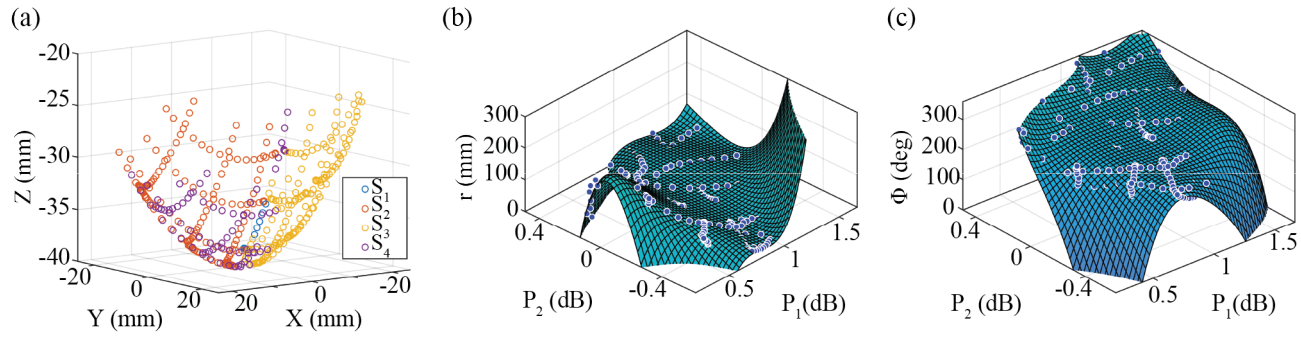

Fig. 6. Robot workspace and surface mapping. a) The responses of the two waveguides results in four sections of the workspace. b) Surface mapping for r. c) Surface mapping for ϕ.

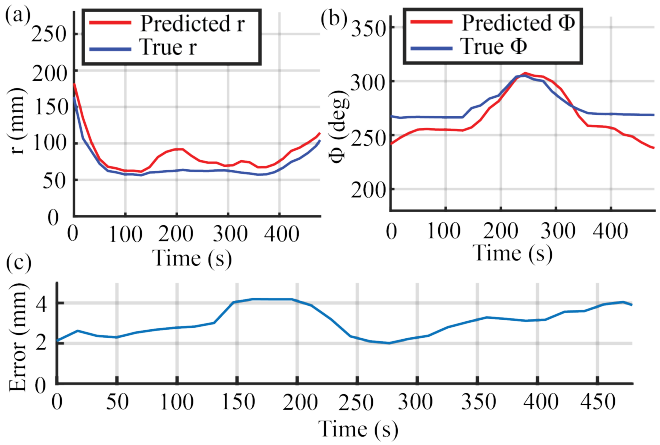

Fig. 7. Continuum robot accuracy testing. A comparison of the predicted and true a) radius of curvature and b) angle ϕ as well as the c) tip position error over time during the experiment, which was 3.08 mm on average, which is 7.7 % of the length of the robot.

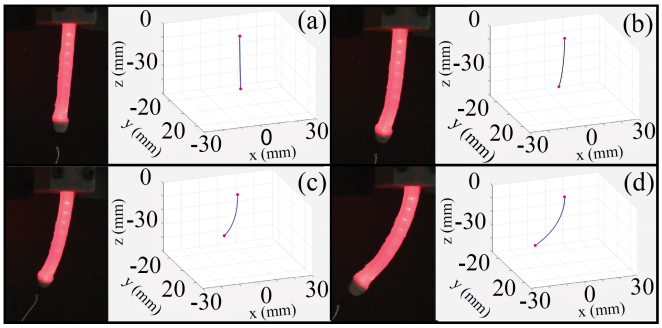

Fig. 8. Real-time shape sensing. a) The robot in its baseline configuration. b-c) The robot is actuated and its curvature (k) increases. d) Keeping k constant, ϕ is increased, resulting in the robot moving closer to the camera.

(Fig. 8, a), the robot was first actuated by keeping ϕ constant, and increasing its curvature k (Fig. 8 b-c), thus decreasing r, according to Eq. 3. Then, the curvature was kept constant, and ϕ was increased, resulting in the robot moving closer to the camera. (Fig. 8 d). The experiment exhibited an accurate prediction of the shape and tip location relative to the observed true position of the robot in space. Please see the accompanying video.

V. Conclusions

We presented a miniaturized 5 mm fully soft continuum robot with functionalized fully soft optical sensor waveguides for shape sensing and tip tracking. We have introduced a laser precision micromaching patterning technique to functionalize tubing to create bidirectional soft optical sensors. We have characterized the patterned cuts effects on the waveguide tubing in bidirectional bending experiments to understand the optical light intensity changes up to large curvatures (i.e., 46.5 m^{-1}). By utilizing constant curvature modeling, in addition to surface mappings based on the two waveguides signals, the system was calibrated to track its shape and tip position. The calibrated workspace was validated through an accuracy experiment that proved the system's capabilities in the 3D space. A GUI was used to display the continuum robot's shape and tip position as it moved through a section of its workspace, allowing for a real-time visualization. The bidirectional response of the waveguides, enabled by the patterning technique, allows for a minimal number of sensors to be required to provide the shape tracking feedback. The reduced number of sensors outputs can lower the computational complexity of the control strategy and simplify system integration. The functionalized tubing represents a low cost, versatile, and simple shape sensing strategy for soft robotic systems, compared to other optical shape sensing approaches, such as FBGs. Our approach allows for a large range of potential applications in soft robotics. The low footprint and compliance of the sensor allow integration into small soft robotic systems, which is beneficial for robots that need to safely navigate in narrow spaces, such as in surgical robotics environments. Future work will focus on optimizing the laser patterning of the waveguides to increase the sensitive range of the robot to have better accuracy when predicting the shape and tip position. Implementation of closed-loop control will be done to allow the robot to not only understand its shape but also move around obstacles in tight spaces and accomplish tasks without the need for manual control.

REFERENCES

[1] J. Zhang, Q. Fang, P. Xiang, D. Sun, Y. Xue, R. Jin, K. Qiu, R. Xiong, Y. Wang, and H. Lu, "A survey on design, actuation, modeling, and control of continuum robot," *Cyborg and Bionic Systems*, vol. 2022, 2022.

[2] S. Li and G. Hao, "Current trends and prospects in compliant continuum robots: A survey," in *Actuators*, vol. 10, no. 7. MDPI, 2021, p. 145.

[3] S. Kolachalama and S. Lakshmanan, "Continuum robots for manipulation applications: A survey," *Journal of Robotics*, vol. 2020, 2020.

[4] R. Kang, E. Guglielmino, L. Zullo, D. T. Branson, I. Godage, and D. G. Caldwell, "Embodiment design of soft continuum robots," *Advances in Mechanical Engineering*, vol. 8, no. 4, p. 1687814016643302, 2016.

[5] D. Rus and M. T. Tolley, "Design, fabrication and control of soft robots," *Nature*, vol. 521, no. 7553, pp. 467–475, 2015.

[6] T. Ashuri, A. Armani, R. Jalilzadeh Hamidi, T. Reasnor, S. Ahmadi, and K. Iqbal, "Biomedical soft robots: Current status and perspective," *Biomedical Engineering Letters*, vol. 10, pp. 369–385, 2020.

[7] C. Lee, M. Kim, Y. J. Kim, N. Hong, S. Ryu, H. J. Kim, and S. Kim, "Soft robot review," *International Journal of Control, Automation and Systems*, vol. 15, pp. 3–15, 2017.

[8] M. Wang, X. Dong, W. Ba, A. Mohammad, D. Axinte, and A. Norton, "Design, modelling and validation of a novel extra slender continuum robot for in-situ inspection and repair in aeroengine," *Robotics and Computer-Integrated Manufacturing*, vol. 67, p. 102054, 2021.

[9] J. L. C. Santiago, I. D. Walker, and I. S. Godage, "Continuum robots for space applications based on layer-jamming scales with stiffening capability," in *2015 IEEE Aerospace Conference*. IEEE, 2015, pp. 1–13.

[10] Y. Yamauchi, Y. Ambe, H. Nagano, M. Konyo, Y. Bando, E. Ito, S. Arnold, K. Yamazaki, K. Itoyama, T. Okatani *et al.*, "Development of a continuum robot enhanced with distributed sensors for search and rescue," *Robomech Journal*, vol. 9, no. 1, pp. 1–13, 2022.

[11] G. Qin, A. Ji, Y. Cheng, W. Zhao, H. Pan, S. Shi, and Y. Song, "A snake-inspired layer-driven continuum robot," *Soft Robotics*, vol. 9, no. 4, pp. 788–797, 2022.

[12] M. M. Coad, L. H. Blumenschein, S. Cutler, J. A. R. Zepeda, N. D. Naclerio, H. El-Hussieny, U. Mehmood, J.-H. Ryu, E. W. Hawkes, and A. M. Okamura, "Vine robots," *IEEE Robotics & Automation Magazine*, vol. 27, no. 3, pp. 120–132, 2019.

[13] M. Wang, L. Du, J. Yuan, S. Ma, and S. Bao, "A bio-inspired continuum robot for out-pipe climbing and confined space navigating," in *2021 IEEE International Conference on Robotics and Biomimetics (ROBIO)*. IEEE, 2021, pp. 74–79.

[14] A. Mehrkish and F. Janabi-Sharifi, "A comprehensive grasp taxonomy of continuum robots," *Robotics and Autonomous Systems*, vol. 145, p. 103860, 2021.

[15] J. Zhang, J. Shi, J. Huang, Q. Wu, Y. Zhao, J. Yang, H. Rajabi, Z. Wu, H. Peng, and J. Wu, "In situ reconfigurable continuum robot with varying curvature enabled by programmable tensegrity building blocks," *Advanced Intelligent Systems*, p. 2300048, 2023.

[16] M. Zhu, S. Biswas, S. I. Dinulescu, N. Kastor, E. W. Hawkes, and Y. Visell, "Soft, wearable robotics and haptics: Technologies, trends, and emerging applications," *Proceedings of the IEEE*, vol. 110, no. 2, pp. 246–272, 2022.

[17] Z. Peng and J. Huang, "Soft rehabilitation and nursing-care robots: A review and future outlook," *Applied Sciences*, vol. 9, no. 15, p. 3102, 2019.

[18] P. H. Nguyen and W. Zhang, "Design and computational modeling of fabric soft pneumatic actuators for wearable assistive devices," *Scientific reports*, vol. 10, no. 1, p. 9638, 2020.

[19] P. E. Dupont, N. Simaan, H. Choset, and C. Rucker, "Continuum robots for medical interventions," *Proceedings of the IEEE*, vol. 110, no. 7, pp. 847–870, 2022.

[20] M. Runciman, A. Darzi, and G. P. Mylonas, "Soft robotics in minimally invasive surgery," *Soft robotics*, vol. 6, no. 4, pp. 423–443, 2019.

[21] M. Cianchetti, T. Ranzani, G. Gerboni, T. Nanayakkara, K. Althoefer, P. Dasgupta, and A. Menciassi, "Soft robotics technologies to address shortcomings in today's minimally invasive surgery: the stiff-flop approach," *Soft robotics*, vol. 1, no. 2, pp. 122–131, 2014.

[22] M. Russo, S. M. H. Sadati, X. Dong, A. Mohammad, I. D. Walker, C. Bergeles, K. Xu, and D. A. Axinte, "Continuum robots: an overview," *Advanced Intelligent Systems*, p. 2200367, 2023.

[23] H. Alfalahi, F. Renda, and C. Stefanini, "Concentric tube robots for minimally invasive surgery: Current applications and future opportunities," *IEEE Transactions on Medical Robotics and Bionics*, vol. 2, no. 3, pp. 410–424, 2020.

[24] T. da Veiga, J. H. Chandler, P. Lloyd, G. Pittiglio, N. J. Wilkinson, A. K. Hoshiar, R. A. Harris, and P. Valdastri, "Challenges of continuum robots in clinical context: a review," *Progress in Biomedical Engineering*, vol. 2, no. 3, p. 032003, 2020.

[25] J. Zhu, L. Lyu, Y. Xu, H. Liang, X. Zhang, H. Ding, and Z. Wu, "Intelligent soft surgical robots for next-generation minimally invasive surgery," *Advanced Intelligent Systems*, vol. 3, no. 5, p. 2100011, 2021.

[26] G. Gerboni, T. Ranzani, A. Diodato, G. Ciuti, M. Cianchetti, and A. Menciassi, "Modular soft mechatronic manipulator for minimally invasive surgery (mis): overall architecture and development of a fully integrated soft module," *Meccanica*, vol. 50, pp. 2865–2878, 2015.

[27] H. Wang, R. Zhang, W. Chen, X. Wang, and R. Pfeifer, "A cable-driven soft robot surgical system for cardiothoracic endoscopic surgery: preclinical tests in animals," *Surgical endoscopy*, vol. 31, pp. 3152–3158, 2017.

[28] Y. Zhong, L. Hu, and Y. Xu, "Recent advances in design and actuation of continuum robots for medical applications," in *Actuators*, vol. 9, no. 4. MDPI, 2020, p. 142.

[29] J. Burgner-Kahrs, D. C. Rucker, and H. Choset, "Continuum robots for medical applications: A survey," *IEEE Transactions on Robotics*, vol. 31, no. 6, pp. 1261–1280, 2015.

[30] Y. Kim, G. A. Parada, S. Liu, and X. Zhao, "Ferromagnetic soft continuum robots," *Science Robotics*, vol. 4, no. 33, p. eaax7329, 2019.

[31] G. Pittiglio, P. Lloyd, T. da Veiga, O. Onaizah, C. Pompili, J. H. Chandler, and P. Valdastri, "Patient-specific magnetic catheters for atraumatic autonomous endoscopy," *Soft Robotics*, vol. 9, no. 6, pp. 1120–1133, 2022.

[32] N. Ebrahimi, C. Bi, D. J. Cappelleri, G. Ciuti, A. T. Conn, D. Faivre, N. Habibi, A. Hošovskỳ, V. Iacovacci, I. S. Khalil *et al.*, "Magnetic actuation methods in bio/soft robotics," *Advanced Functional Materials*, vol. 31, no. 11, p. 2005137, 2021.

[33] P. Lloyd, O. Onaizah, G. Pittiglio, D. K. Vithanage, J. H. Chandler, and P. Valdastri, "Magnetic soft continuum robots with braided reinforcement," *IEEE Robotics and Automation Letters*, vol. 7, no. 4, pp. 9770–9777, 2022.

[34] H. Wang, M. Totaro, and L. Beccai, "Toward perceptive soft robots: Progress and challenges," *Advanced Science*, vol. 5, no. 9, p. 1800541, 2018.

[35] J. Morrow, H.-S. Shin, C. Phillips-Grafflin, S.-H. Jang, J. Torrey, R. Larkins, S. Dang, Y.-L. Park, and D. Berenson, "Improving soft pneumatic actuator fingers through integration of soft sensors, position and force control, and rigid fingernails," in *2016 IEEE international conference on robotics and automation (ICRA)*. IEEE, 2016, pp. 5024–5031.

[36] R. K. Kramer, C. Majidi, R. Sahai, and R. J. Wood, "Soft curvature sensors for joint angle proprioception," in *2011 IEEE/RSJ International Conference on Intelligent Robots and Systems*. IEEE, 2011, pp. 1919–1926.

[37] V. Wall, G. Zöller, and O. Brock, "A method for sensorizing soft actuators and its application to the rbo hand 2," in *2017 IEEE International Conference on Robotics and Automation (ICRA)*. IEEE, 2017, pp. 4965–4970.

[38] S. Russo, T. Ranzani, H. Liu, S. Nefti-Meziani, K. Althoefer, and A. Menciassi, "Soft and stretchable sensor using biocompatible electrodes and liquid for medical applications," *Soft robotics*, vol. 2, no. 4, pp. 146–154, 2015.

[39] S.-H. Zhang, F.-X. Wang, J.-J. Li, H.-D. Peng, J.-H. Yan, and G.-B. Pan, "Wearable wide-range strain sensors based on ionic liquids and monitoring of human activities," *Sensors*, vol. 17, no. 11, p. 2621, 2017.

[40] T. Helps and J. Rossiter, "Proprioceptive flexible fluidic actuators using conductive working fluids," *Soft robotics*, vol. 5, no. 2, pp. 175–189, 2018.

[41] M. Totaro, A. Mondini, A. Bellacicca, P. Milani, and L. Beccai, "Integrated simultaneous detection of tactile and bending cues for soft robotics," *Soft robotics*, vol. 4, no. 4, pp. 400–410, 2017.

[42] K. Kure, T. Kanda, K. Suzumori, and S. Wakimoto, "Flexible displacement sensor using injected conductive paste," *Sensors and Actuators A: Physical*, vol. 143, no. 2, pp. 272–278, 2008.

[43] H. A. Wurdemann, S. Sareh, A. Shafti, Y. Noh, A. Faragasso, D. S. Chathuranga, H. Liu, S. Hirai, and K. Althoefer, "Embedded electro-

conductive yarn for shape sensing of soft robotic manipulators," in *2015 37th Annual International Conference of the IEEE Engineering in Medicine and Biology Society (EMBC)*. IEEE, 2015, pp. 8026–8029.

[44] J. Zhao and A. Abbas, "A low-cost soft coiled sensor for soft robots," in *Dynamic Systems and Control Conference*, vol. 50701. American Society of Mechanical Engineers, 2016, p. V002T26A006.

[45] A. Pagoli, F. Chapelle, J.-A. Corrales-Ramon, Y. Mezouar, and Y. Lapusta, "Large-area and low-cost force/tactile capacitive sensor for soft robotic applications," *Sensors*, vol. 22, no. 11, p. 4083, 2022.

[46] B. Aksoy, Y. Hao, G. Grasso, K. M. Digumarti, V. Cacucciolo, and H. Shea, "Shielded soft force sensors," *Nature Communications*, vol. 13, no. 1, p. 4649, 2022.

[47] W. R. Johnson, J. Booth, and R. Kramer-Bottiglio, "Integrated sensing in robotic skin modules," in *2021 IEEE Sensors*. IEEE, 2021, pp. 1–4.

[48] T. Hellebrekers, O. Kroemer, and C. Majidi, "Soft magnetic skin for continuous deformation sensing," *Advanced Intelligent Systems*, vol. 1, no. 4, p. 1900025, 2019.

[49] Y. Yan, Z. Hu, Z. Yang, W. Yuan, C. Song, J. Pan, and Y. Shen, "Soft magnetic skin for super-resolution tactile sensing with force self-decoupling," *Science Robotics*, vol. 6, no. 51, p. eabc8801, 2021.

[50] M. D. Mitchell, F. E. Hurley, and C. D. Onal, "Fast probabilistic 3-d curvature proprioception with a magnetic soft sensor," in *2021 IEEE 17th International Conference on Automation Science and Engineering (CASE)*. IEEE, 2021, pp. 215–220.

[51] M. Luo, E. H. Skorina, W. Tao, F. Chen, S. Ozel, Y. Sun, and C. D. Onal, "Toward modular soft robotics: Proprioceptive curvature sensing and sliding-mode control of soft bidirectional bending modules," *Soft robotics*, vol. 4, no. 2, pp. 117–125, 2017.

[52] J. Hao, Z. Zhang, S. Wang, and C. Shi, "2d shape estimation of a pneumatic-driven soft finger with a large bending angle based on learning from two sensing modalities," *Advanced Intelligent Systems*, p. 2200324, 2023.

[53] O. Al-Ahmad, M. Ourak, J. Van Roosbroeck, J. Vlekken, and E. Vander Poorten, "Improved fbg-based shape sensing methods for vascular catheterization treatment," *IEEE Robotics and Automation Letters*, vol. 5, no. 3, pp. 4687–4694, 2020.

[54] K. C. Galloway, Y. Chen, E. Templeton, B. Rife, I. S. Godage, and E. J. Barth, "Fiber optic shape sensing for soft robotics," *Soft robotics*, vol. 6, no. 5, pp. 671–684, 2019.

[55] I. Floris, J. M. Adam, P. A. Calderón, and S. Sales, "Fiber optic shape sensors: A comprehensive review," *Optics and Lasers in Engineering*, vol. 139, p. 106508, 2021.

[56] R. A. Shaik and E. Rufus, "Recent trends and role of large area flexible electronics in shape sensing application–a review," *Industrial Robot: the international journal of robotics research and application*, vol. 48, no. 5, pp. 745–762, 2021.

[57] J. Guo, C. Yang, Q. Dai, and L. Kong, "Soft and stretchable polymeric optical waveguide-based sensors for wearable and biomedical applications," *Sensors*, vol. 19, no. 17, p. 3771, 2019.

[58] C. Wu, X. Liu, and Y. Ying, "Soft and stretchable optical waveguide: light delivery and manipulation at complex biointerfaces creating unique windows for on-body sensing," *ACS sensors*, vol. 6, no. 4, pp. 1446–1460, 2021.

[59] S. Sareh, Y. Noh, M. Li, T. Ranzani, H. Liu, and K. Althoefer, "Macrobend optical sensing for pose measurement in soft robot arms," *Smart Materials and Structures*, vol. 24, no. 12, p. 125024, 2015.

[60] H. Zhao, K. O'brien, S. Li, and R. F. Shepherd, "Optoelectronically innervated soft prosthetic hand via stretchable optical waveguides," *Science robotics*, vol. 1, no. 1, p. eaai7529, 2016.

[61] S. Sareh, A. Jiang, A. Faragasso, Y. Noh, T. Nanayakkara, P. Dasgupta, L. D. Seneviratne, H. A. Wurdemann, and K. Althoefer, "Bio-inspired tactile sensor sleeve for surgical soft manipulators," in *2014 IEEE International Conference on Robotics and Automation (ICRA)*. IEEE, 2014, pp. 1454–1459.

[62] M. McCandless, A. Gerald, A. Carroll, H. Aihara, and S. Russo, "A soft robotic sleeve for safer colonoscopy procedures," *IEEE robotics and automation letters*, vol. 6, no. 3, pp. 5292–5299, 2021.

[63] L. Mo, D. Zhang, X. Fu, J. Dou, K. Li, L. Bai, Y. Bai, Q. Zhang, and X. Zhao, "A multidirectional external perception soft actuator based on flexible optical waveguide for underwater teleoperation," *Advanced Intelligent Systems*, p. 2300029, 2023.

[64] B. Merillas, J. Martín-de León, F. Villafañe, and M. Á. Rodríguez-Pérez, "Optical properties of polyisocyanurate–polyurethane aerogels: Study of the scattering mechanisms," *Nanomaterials*, vol. 12, no. 9, p. 1522, 2022.

[65] W. Zhang, H. Jia, L. Ju, Y. Shi, X. Ding, and Y. Feng, "Bending-sensitive optical waveguide sensor with carbon-fiber layer for monitoring grip strength," *IEEE Transactions on Neural Systems and Rehabilitation Engineering*, vol. 31, pp. 1922–1932, 2023.

[66] R. J. Webster III and B. A. Jones, "Design and kinematic modeling of constant curvature continuum robots: A review," *The International Journal of Robotics Research*, vol. 29, no. 13, pp. 1661–1683, 2010.

[67] M. McCandless, F. J. Wise, and S. Russo, "A soft robot with three dimensional shape sensing and contact recognition multi-modal sensing via tunable soft optical sensors," in *2023 IEEE International Conference on Robotics and Automation (ICRA)*. IEEE, 2023, pp. 573–580.